

14.4 Some Potentially Interesting Differences in the Midlevel Kinematic Characteristics of a Nontornadic and Tornadoic Supercell Observed by ELDORA during VORTEX

PAUL MARKOWSKI*

Department of Meteorology, Pennsylvania State University, University Park, PA

1. Introduction

Downdrafts are widely believed to be important for the formation of tornadoes within supercells in the absence of preexisting near-ground vertical vorticity (Davies-Jones 1982; Walko 1993; Xue 2004), and the relative coldness of downdrafts is increasingly believed to be related to the likelihood of tornadogenesis within a supercell. Recent surface observations obtained by mobile mesonets have revealed that the outflow of rear-flank downdrafts (RFDs) associated with tornadoic supercells have been found, on average, to have surface virtual potential temperature (θ_v) perturbations approximately 3–5 K warmer than the RFDs associated with nontornadoic supercells (Markowski et al. 2002; Grzych et al. 2006). Idealized numerical simulations have suggested that near-surface angular momentum convergence might be facilitated by increasingly buoyant downdraft properties (Markowski et al. 2003). Furthermore, the RFD outflow associated with nontornadoic supercells generally also has been associated with significant equivalent potential temperature (θ_e) deficits (typically >10 K), with midlevel, environmental θ_e values commonly being detected at the surface. The RFD outflow of supercells that produce significant tornadoes has tended to contain smaller (occasionally negligible) θ_e deficits at the surface (Markowski et al. 2002).

Given the apparent relationship between the intensification of near-ground rotation in supercells and the thermodynamic properties of the RFD outflow that tends to closely accompany the development of near-ground rotation, the processes that influence the thermodynamic properties of RFD outflow are naturally of interest. Although a considerable fraction of the variance of thermodynamic characteristics at the surface within RFD outflow has been found to be tied to the ambient low-level relative humidity [e.g., Markowski et al. (2002) documented a linear correlation of ~ 0.6 between the surface temperature deficit in the RFD outflow and the dewpoint depression in the near-storm inflow], one might also reasonably expect a priori that downdraft characteristics ought to depend, at least in part, on the characteristics of the midlevel flow (e.g., perhaps the strength of midlevel storm-relative winds and the degree to which they penetrate the updraft). Therefore, it might be worthwhile to investigate differences in the midlevel kinematic characteristics of nontornadoic and tornadoic supercells.

In this preprint, the midlevel kinematic characteristics of two supercell thunderstorms observed during the Verification of the Origins of Tornadoes Experiment (VORTEX; Rasmussen

et al. 1994), one tornadoic and the other nontornadoic [the 16 May 1995 and 12 May 1995 cases, respectively; refer to Wakimoto et al. (1998) and Wakimoto and Cai (2000) for synoptic overviews of these cases], are compared using airborne dual-Doppler wind retrievals. Considerable similarity has been documented in the low-level kinematic fields resolvable by airborne dual-Doppler wind observations in prior studies of these two storms (Wakimoto and Liu 1998; Wakimoto et al. 1998; Wakimoto and Cai 2000), although less similarity in the RFD outflow characteristics (e.g., outflow buoyancy and equivalent potential temperature) of these two storms has been documented (Markowski et al. 2002). The underlying challenge in comparing tornadoic and nontornadoic cases is that there are bound to be nearly innumerable differences between any two cases; it is therefore difficult to know whether any particular difference between two cases has any relevance to tornadogenesis.

2. Data and methodology

Data from the Electra Doppler Radar (ELDORA) system on the National Center for Atmospheric Research (NCAR) Electra aircraft (Hildebrand et al. 1994) were objectively analyzed to a $40 \times 40 \times 18$ km Cartesian grid having horizontal and vertical grid spacings of 400 m and 500 m, respectively, using the technique described by Barnes (1964). A smoothing parameter of $\kappa = 0.37$ km² was used, and data farther than 1.3 km from a grid point [which corresponds to $(5\kappa)^{1/2}$] had their weights set to zero in the interest of computational expediency. No extrapolation of the observations was permitted in the assignment of grid values, as is commonly permitted (variational wind synthesis techniques like that used herein seem to be able to perform well even if there are missing values assigned to grid points near domain boundaries—most notably near the ground—due to the forbiddance of extrapolation). The effects of storm translation also were accounted for in the objective analysis by considering the mean storm motions estimated by Wakimoto and Cai (2000) (12 May 1995) and Wakimoto et al. (1998) (16 May 1995).

The three-dimensional wind synthesis was performed using the variational technique with weak constraints presented by Gamache (1997) [this method is fairly similar to that described by Gao et al. (1999)]. The three components of the wind field are obtained by minimizing a cost function that considers the radial velocity projections, anelastic mass continuity, upper and lower boundary conditions, and degree of smoothing [see Gamache (1997) for further details]. Precipitation fall speeds were parameterized in terms of radar reflectivity fac-

*Corresponding author address: Dr. Paul Markowski, Department of Meteorology, Pennsylvania State University, 503 Walker Building, University Park, PA 16802; e-mail: pmarkowski@psu.edu.

tor using the parameterization used by Dowell and Bluestein (2002). The reader is referred to Jorgensen et al. (1983), Hildebrand and Mueller (1985), Ray and Stephenson (1990), and Wakimoto et al. (1998) for general discussions of the errors in airborne dual-Doppler wind retrievals.

3. Observations

Horizontal wind vector fields are presented at 3 km and 5 km above ground level (AGL) at two times on 12 May 1995 and 16 May 1995: one time is 17–18 min prior to the time of tornadogenesis (in the case of 16 May 1995 tornadic supercell) or the time of maximum low-level rotation (in the case of the 12 May 1995 nontornadic supercell) (Fig. 1), and the other time coincides with the time of tornadogenesis or time of maximum low-level rotation (Fig. 2). One rather obvious difference between the 12 May and 16 May cases at midlevels is that a pronounced westerly “jet” is present to the rear of the storm in the 12 May case (e.g., Figs. 1a and 2a). The jet contains westerly storm-relative winds in excess of 20 m s^{-1} and appears to be very similar to that which Bluestein and Gaddy (2001) documented in the 22 May 1995 nontornadic supercell observed during VORTEX. This region of “rear inflow” is associated with erosion of the radar echo (Figs. 1a), seemingly similar to what Nelson (1977) observed in a nontornadic supercell occurring in the central Oklahoma Doppler radar network on 25 May 1974. In contrast, there is virtually no significant rear-to-front storm-relative wind component at 3 km or 5 km AGL in the 16 May 1995 tornadic supercell (Figs. 1b,d and 2b,d). In fact, the direction of the storm-relative wind a few kilometers to the northwest of the low-level circulation center differs by nearly 180° compared to the 12 May case.

The midlevel “rear-inflow jet” in the 12 May 1995 nontornadic supercell appears to be related to a significant region of anticyclonic vertical vorticity (Fig. 4a). The magnitude of the midlevel negative vertical vorticity in the 12 May storm ($>1.5 \times 10^{-2} \text{ s}^{-1}$) is roughly three times that observed in the 16 May case, and the circulation differences are even greater given the fact that the negative vorticity region is much larger in the 12 May storm than in the 16 May storm. (Curiously, the 12 May nontornadic supercell also has approximately 1.5–2.5 times as much cyclonic circulation at low- and midlevels than the 16 May tornadic supercell, depending on the circulation curve chosen.) Bluestein and Gaddy (2001) also noted a strong midlevel anticyclone in conjunction with the westerly jet that they observed.

Comparison of the environmental hodographs from the two cases probably would not lead one to anticipate such differences in the midlevel storm-relative wind fields (Fig. 3). The storm-relative winds at 3 km (5 km) AGL differ by approximately 30° and 5 m s^{-1} (10° and 2 m s^{-1}). Clearly internal storm dynamical processes were important in leading to the midlevel, storm-scale flow differences, e.g., the 12 May hodograph (Fig. 3) certainly was not suggestive of strong storm-relative flow from the rear (e.g., Fig. 1a). Of course, differences in the midlevel kinematic fields resulting from differences in internal storm dynamical processes ultimately *must* depend on the hodograph, at least in part (i.e., storm structure depends on the storm environment), but not necessarily on only the mi-

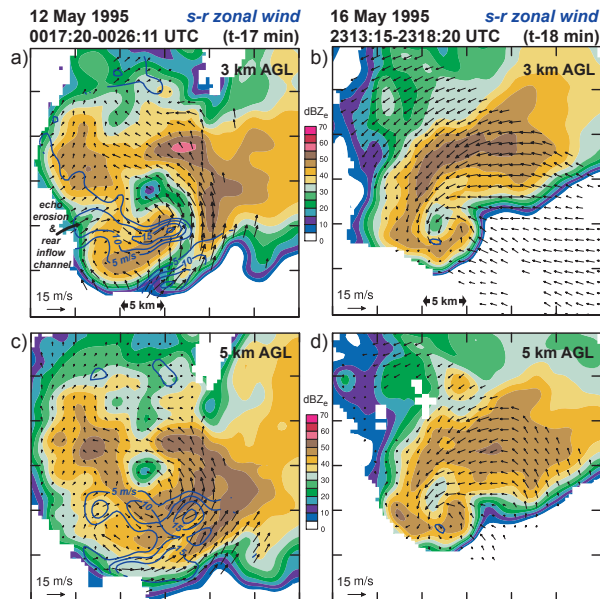


FIG. 1. (a) Horizontal cross-section of equivalent radar reflectivity factor (color shaded; see legend), zonal storm-relative (s-r) wind component (5 m s^{-1} intervals, starting at 5 m s^{-1}), and storm-relative wind vectors at 3 km AGL for the 0017:20–0026:11 UTC wind synthesis on 12 May 1995 (roughly 17 min before the time of strongest low-level rotation). (b) As in (a), but for the 2313:15–2318:20 UTC wind synthesis on 16 May 1995 (roughly 18 min before tornadogenesis). (c)–(d) As in (a)–(b), respectively, but at 5 km AGL.

dlevel portion of the hodograph, and the relationship between storm structure and storm environment is horribly nonlinear.

The VORTEX mobile mesonet observed θ_v deficits of nearly 7 K within the outflow of the 12 May nontornadic supercell in the immediate vicinity of its low-level circulation center, and deficits exceeding 8 K in the trailing portion of the hook echo, during the time of maximum low-level rotation (Fig. 5a). Tornadogenesis occurred prior to the arrival of the mobile mesonet in the 16 May case, but in the period approximately 7–17 min after tornadogenesis (during which time a tornado was in progress), the mobile mesonet marginally sampled the RFD outflow south of the tornado. The mobile mesonet observed θ_v deficits in excess of 4 K there (Fig. 5b). With regards to θ_e , deficits in excess of 15 K and 8 K were observed in the portions of the RFD outflow sampled by the mobile mesonet on 12 May and 16 May, respectively (Fig. 6). The minimum θ_e values observed at the surface in the 12 May and 16 May cases were similar to those found at altitudes of 2.2 km and 1.3 km AGL, respectively, on proximity soundings obtained near the storms.

Although the mobile mesonet sampling was not ideal, what limited observations are available suggest that the rear-flank downdraft outflow was more negatively buoyant in the 12 May nontornadic case compared to the 16 May tornadic case. One might speculate that the midlevel, rear-inflow jet observed in the 12 May storm, which appears to be associated with substantial entrainment of midlevel (and potentially cold) environmental air, played a role in promoting the relatively cold outflow. The boundary layer relative humidity was actually somewhat smaller in the inflow of the 12 May supercell compared

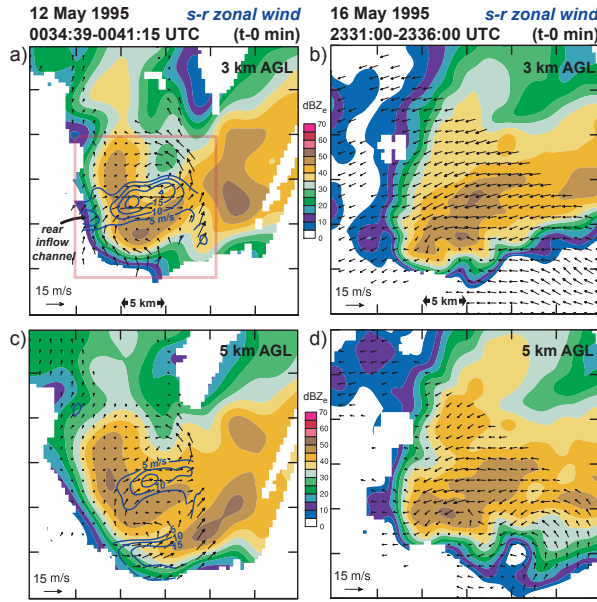


FIG. 2. As in Fig. 1, but for the 0034:39–00:41:15 UTC wind synthesis on 12 May 1995 (the time of strongest low-level rotation) and 0031:00–00:36:00 UTC wind synthesis on 16 May 1995 (the time of tornadogenesis). The red square in (a) encloses the region depicted in Figs. 5a and 6a.

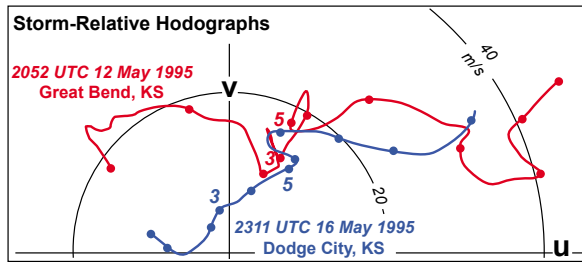


FIG. 3. Storm-relative hodographs obtained from the environments of the 12 May 1995 (red) and 16 May 1995 (blue) supercells. Dots are placed along the hodographs at 1 km intervals. The 3 and 5 km AGL elevations are indicated with numerals. Adapted from Wakimoto et al. (1998) and Wakimoto and Cai (2000).

to 16 May supercell; thus, subcloud layer evaporative cooling actually would have been greater in the 16 May case given an identical hydrometeor distribution as in the 12 May case. [This is *not* a good assumption, however. In fact, Wakimoto and Cai (2000) actually made a point to note the more extensive radar echo in the RFD region in the 12 May storm compared to the 16 May storm, although radar reflectivity is generally not a good measure of hydrometeor size distribution and evaporative cooling potential.] Finally, it might be noteworthy that the 22 May 1995 nontornadic supercell observed during VORTEX, mentioned earlier as having a similar midlevel, rear-inflow jet as that observed in the 12 May 1995 supercell, also was revealed by the mobile mesonet to be accompanied by relatively cold RFD outflow at the surface.

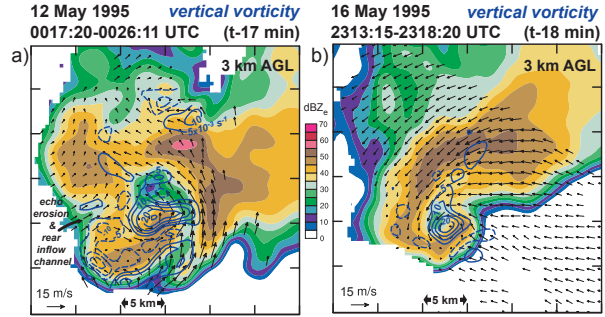


FIG. 4. As in Fig. 1, but vertical vorticity is contoured ($5 \times 10^{-3} \text{ s}^{-1}$ intervals, negative contours dashed, 0 s^{-1} contour suppressed for clarity).

4. Final comments and future work

It is difficult to say how common or significant these observations of midlevel rear-inflow jets are, given the relative scarcity of both observed and simulated three-dimensional wind fields of supercell thunderstorms. In the small sample (roughly a dozen) of VORTEX supercells, the rear-inflow jet appears to have been observed at least twice, both times in nontornadic supercells (22 May 1995 is the other occasion; Bluestein and Gaddy 2001). A survey of past dual-Doppler wind syntheses of supercell thunderstorms published in the literature (e.g., Ray 1975; Brandes 1977, 1981; Heymsfield 1978)—neither tornadic nor nontornadic—does not reveal similar rear-inflow jets at midlevels, nor do numerical simulation studies (e.g., Klemp et al. 1981), at least when such midlevel kinematic fields are presented. Although it seems likely that there are a multitude of tornadogenesis failure modes, perhaps the presence of a strong midlevel rear-inflow jet is one such failure mode, and might indicate that excessive midlevel entrainment of environmental air (midlevel environmental air typically is quite potentially cold, especially in the Great Plains region) will be detrimental to tornadogenesis by promoting excessively cold outflow at the surface. At the very least, the observations presented herein indicate that a model of supercell airflow that is predominantly determined by the environmental storm-relative winds deduced from a nearby hodograph, such as that presented by Browning (1964; his Fig. 2), may be too simple on some occasions, owing to significant accelerations induced by highly nonlinear, internal storm-scale dynamics (which again, are not independent of the hodograph, but our current level of understanding does not allow us to anticipate what these effects will be based on inspection of the hodograph).

In the future I believe it might be worthwhile to explore the formation of the midlevel jet and negative vorticity anomaly, either with a more thorough analysis of the observations and/or numerical simulations, the latter of which might also be useful for trying to establish a relationship, if one exists, between midlevel kinematics and low-level thermodynamics. The low-level thermodynamic properties of supercells are increasingly believed to be important to tornadogenesis (e.g., Markowski et al. 2002, 2003; Grzych et al. 2006). Although low-level thermodynamics are notoriously difficult to observe, perhaps in some cases they can be inferred from the kinematic characteristics aloft (at least in a qualitative sense with sufficient skill

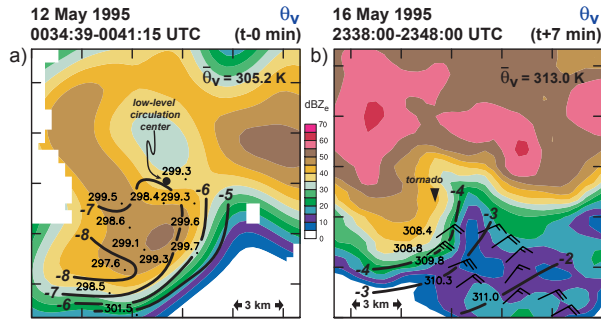


FIG. 5. (a) Horizontal cross-section of equivalent radar reflectivity factor at 1 km AGL (color shaded; see legend), mobile mesonet station models, and contours of virtual potential temperature perturbation, θ'_v (1 K intervals) for the 0034:39–0041:15 UTC period on 12 May 1995 (the time of strongest low-level rotation). Station models display virtual potential temperature, θ_v . Wind data are missing from the station models. The ambient virtual potential temperature of the inflow environment, $\bar{\theta}_v$, also is indicated. The red square in Fig. 2(a) encloses the domain displayed above. (b) As in (a), but for the 2338:00–2348:00 UTC period on 16 May 1995 (the tornado is in progress). Wind barbs are storm-relative. The radar data are from the Dodge City NWS radar (KDDC).

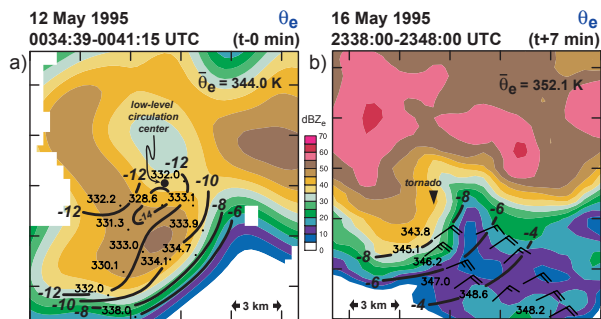


FIG. 6. As in Fig. 5, but equivalent potential temperature (θ_e), its perturbations (θ'_e), and its ambient value ($\bar{\theta}_e$) are displayed instead.

to be of use to nowcasters), which are likely to be more easily observable in general. Finally, the observations documented herein might highlight the importance of sampling entire storm volumes in future field experiments, including regions of the storm that, at first glance, might seem too far removed from the tornadic region to be relevant to tornadogenesis.

Acknowledgments. I wish to thank Roger Wakimoto, Hanne Murphey, and Huaqing Cai for graciously providing their edited ELDORA data, John Gamache for sharing his variational wind synthesis technique and code, and Yvette Richardson, David Dowell, Josh Wurman, Jerry Straka, Erik Rasmussen, and Bob Davies-Jones for their insight and ongoing discussions pertaining to supercell thunderstorms and tornadogenesis. Support from NSF grant ATM-0338661 also is acknowledged.

REFERENCES

Barnes, S. L., 1964: A technique for maximizing details in numerical weather map analysis. *J. Appl. Meteor.*, **3**, 396–409.

Bluestein, H. B., and S. G. Gaddy, 2001: Airborne pseudo-dual-Doppler analysis of a rear-inflow jet and deep convergence zone within a supercell. *Mon. Wea. Rev.*, **129**, 2270–2289.

Brandes, E. A., 1977: Flow in a severe thunderstorm observed by dual-Doppler radar. *Mon. Wea. Rev.*, **105**, 113–120.

Brandes, E. A., 1981: Finestructure of the Del City-Edmond tornadic mesocirculation. *Mon. Wea. Rev.*, **109**, 635–647.

Browning, K. A., 1964: Airflow and precipitation trajectories within severe local storms which travel to the right of the winds. *J. Atmos. Sci.*, **21**, 634–639.

Davies-Jones, R. P., 1982: A new look at the vorticity equation with application to tornadogenesis. Preprints, *12th Conf. on Severe Local Storms*, San Antonio, TX, Amer. Meteor. Soc., 249–252.

Dowell, D. C., and H. B. Bluestein, 2002: The 8 June 1995 McLean, Texas storm. Part I: Observations of cyclic tornadogenesis. *Mon. Wea. Rev.*, **130**, 2626–2648.

Gamache, J. F., 1997: Evaluation of a fully three-dimensional variational Doppler analysis technique. Preprints, *28th Conf. on Radar Meteorology*, Austin, TX, Amer. Meteor. Soc., 422–423.

Gao, J., M. Xue, A. Shapiro, and K. K. Droegemeier, 1999: A variational method for the analysis of three-dimensional wind fields from two Doppler radars. *Mon. Wea. Rev.*, **127**, 2128–2142.

Grzych, M. L., B. D. Lee, and C. A. Finley, 2006: Thermodynamic analysis of supercell rear-flank downdrafts from Project AN-SWERS. *Mon. Wea. Rev.*, **134**, in press.

Heysmsfield, G. M., 1978: Kinematic and dynamic aspects of the Harrah tornadic storm analyzed from dual-Doppler radar data. *Mon. Wea. Rev.*, **106**, 233–254.

Hildebrand, P. H., and C. K. Mueller, 1985: Evaluation of meteorological airborne Doppler radar. Part I: Dual-Doppler analyses of air motions. *J. Atmos. Oceanic Technol.*, **2**, 362–380.

Hildebrand, P. H., C. A. Walther, C. L. Frush, J. Testud, and F. Baudin, 1994: The ELDORA/ASTRAIA airborne Doppler weather radar: Goals, design, and first field tests. *Proc. IEEE*, **82**, 1873–1890.

Jorgensen, D. P., P. H. Hildebrand, and C. L. Frush, 1983: Feasibility test of an airborne pulse-Doppler meteorological radar. *J. Appl. Meteor.*, **22**, 744–757.

Klemp, J. B., R. B. Wilhelmson, and P. S. Ray, 1981: Observed and numerically simulated structure of a mature supercell thunderstorm. *J. Atmos. Sci.*, **38**, 1558–1580.

Markowski, P. M., J. M. Straka, and E. N. Rasmussen, 2002: Direct surface thermodynamic observations within the rear-flank downdrafts of nontornadic and tornadic supercells. *Mon. Wea. Rev.*, **130**, 1692–1721.

Markowski, P. M., J. M. Straka, and E. N. Rasmussen, 2003: Tornadogenesis resulting from the transport of circulation by a downdraft. *J. Atmos. Sci.*, **60**, 795–823.

Nelson, S. P., 1977: Rear flank downdraft: A hailstorm intensification mechanism. Preprints, *10th Conf. on Severe Local Storms*, Omaha, Amer. Meteor. Soc., 521–525.

Rasmussen, E. N., J. M. Straka, R. P. Davies-Jones, C. A. Doswell, F. H. Carr, M. D. Eilts, and D. R. MacGorman, 1994: Verification of the Origins of Rotation in Tornadoes Experiment: VORTEX. *Bull. Amer. Meteor. Soc.*, **75**, 995–1006.

Ray, P. S., and M. Stephenson, 1990: Assessment of the geometric and temporal errors associated with airborne Doppler radar measurements of a convective storm. *J. Atmos. Oceanic Technol.*, **7**, 206–217.

Ray, P. S., R. J. Doviak, G. B. Walker, D. Sirmans, J. Carter, and B. Bumgarner, 1975: Dual-Doppler observation of a tornadic storm. *J. Appl. Meteor.*, **14**, 1521–1530.

- Walko, R. L., 1993: Tornado spin-up beneath a convective cell: Required basic structure of the near-field boundary layer winds. *The Tornado: Its Structure, Dynamics, Prediction, and Hazards*, Geophys. Monogr., No. 79, Amer. Geophys. Union, 89–95.
- Wakimoto, R. M., and C. Liu, 1998: The Garden City, Kansas, storm during VORTEX 95. Part II: The wall cloud and tornado. *Mon. Wea. Rev.*, **126**, 393–408.
- Wakimoto, R. M., and H. Cai, 2000: Analysis of a nontornadic storm during VORTEX 95. *Mon. Wea. Rev.*, **128**, 565–592.
- Wakimoto, R. M., C. Liu, and H. Cai, 1998: The Garden City, Kansas, storm during VORTEX 95. Part I: Overview of the storm life cycle and mesocyclogenesis. *Mon. Wea. Rev.*, **126**, 372–392.
- Xue, M., 2004: Tornadogenesis within a simulated supercell storm. Preprints, *22nd Conf. on Severe Local Storms*, Hyannis, MA, Amer. Meteor. Soc.